Molecular dynamics-based identification of binding pathways and two distinct high-affinity sites for succinate in succinate receptor 1/GPR91

Shenol, Aslihan; Lückmann, Michael; Trauelsen, Mette; Lambrughi, Matteo; Tiberti, Matteo; Papaleo, Elena; Frimurer, Thomas M.; Schwartz, Thue W.

Published in:
Molecular Cell

Link to article, DOI:
10.1016/j.molcel.2024.01.011

Publication date:
2024

Document Version
Publisher's PDF, also known as Version of record

Molecular Cell

Article

Molecular dynamics-based identification of binding pathways and two distinct high-affinity sites for succinate in succinate receptor 1/GPR91

Graphical abstract

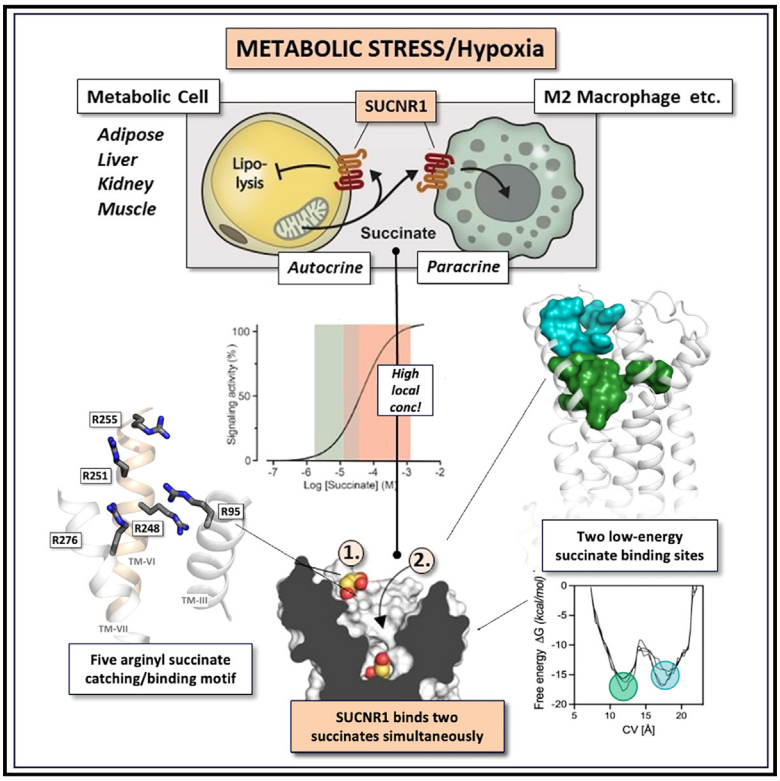

Highlights

- SUCNR1 attracts and binds succinate through a cluster of arginines around TM-VI
- The arginines constitute two low-energy succinate binding sites
- SUCNR1 is activated by simultaneous binding of two succinates at high concentrations
- Binding of succinate, but not antagonist, unlocks constrained ECL-2 via water cluster

Authors

Aslihan Shenol, Michael Lückmann, Mette Trauelsen, ..., Elena Papaleo, Thomas M. Frimurer, Thue W. Schwartz

Correspondence

tws@sund.ku.dk

In brief

Extracellular succinate is an auto- and paracrine metabolic stress signal sensed by SUCNR1. Using MD simulations, Shenol et al. found that SUCNR1 has two low-energy binding sites, and its selective activation by high, local concentrations of succinate requires simultaneous occupancy of both high-affinity sites.

Shenol et al., 2024, Molecular Cell *84*, 955–966
March 7, 2024
https://doi.org/10.1016/j.molcel.2024.01.011

CellPress

Molecular Cell

CellPress
OPEN ACCESS

Article

Molecular dynamics-based identification of binding pathways and two distinct high-affinity sites for succinate in succinate receptor 1/GPR91

Aslihan Shenol,[1] Michael Lückmann,[1] Mette Trauelsen,[1] Matteo Lambrughi,[2] Matteo Tiberti,[2] Elena Papaleo,[2,3] Thomas M. Frimurer,[1] and Thue W. Schwartz[1,4,*]

[1]Novo Nordisk Foundation Center for Basic Metabolic Research, Faculty of Health and Medical Sciences, University of Copenhagen, Copenhagen, Denmark

[2]Cancer Structural Biology, Danish Cancer Society Research Center, Copenhagen, Denmark

[3]Cancer Systems Biology, Section for Bioinformatics, Department of Health and Technology, Technical University of Denmark, Lyngby, Denmark

[4]Lead contact

*Correspondence: tws@sund.ku.dk

https://doi.org/10.1016/j.molcel.2024.01.011

SUMMARY

SUCNR1 is an auto- and paracrine sensor of the metabolic stress signal succinate. Using unsupervised molecular dynamics (MD) simulations (170.400 ns) and mutagenesis across human, mouse, and rat SUCNR1, we characterize how a five-arginine motif around the extracellular pole of TM-VI determines the initial capture of succinate in the extracellular vestibule (ECV) to either stay or move down to the orthosteric site. Metadynamics demonstrate low-energy succinate binding in both sites, with an energy barrier corresponding to an intermediate stage during which succinate, with an associated water cluster, unlocks the hydrogen-bond-stabilized conformationally constrained extracellular loop (ECL)-2b. Importantly, simultaneous binding of two succinate molecules through either a "sequential" or "bypassing" mode is a frequent endpoint. The mono-carboxylate NF-56-EJ40 antagonist enters SUCNR1 between TM-I and -II and does not unlock ECL-2b. It is proposed that occupancy of both high-affinity sites is required for selective activation of SUCNR1 by high local succinate concentrations.

INTRODUCTION

Key metabolites function as extracellular autocrine and paracrine signals of nutrient availability and metabolic stress. These metabolites are detected by a fascinating group of G-protein coupled receptors (GPCRs) that are molecularly tuned to selectively be activated by the local, high micro- to millimolar concentrations of the metabolites.[1] This study deals with SUCNR1, which as GPR91 was deorphanized in 2004 as a receptor for the tricarboxylic acid cycle (TCA) metabolite, succinate.[2,3] Succinate accumulates in response to metabolic stress, such as hypoxia, due to the reverse action of succinate dehydrogenase[4,5] and is transported out of the mitochondria and out of the cells to be sensed by SUCNR1 expressed both on the metabolically active cell itself and on neighboring, e.g., anti-inflammatory M2 macrophages.[5,6] Thus, through autocrine and paracrine mechanisms, succinate/SUCNR1 signaling is involved in beneficial tissue repair and remodeling, whereas sustained locally elevated succinate may lead to damaging inflammatory reactions through SUCNR1 on, e.g., pro-inflammatory M1 macrophages and activated stellate cells.[5,7] Recently, SUCNR1 sensing of succinate has also been implicated in the control of leptin expression and hyperleptinemia-associated related to obesity.[8] However, the molecular basis for how succinate can bind and activate SUCNR1 with high selectivity albeit low potency is unclear.

A large number of ligand binding sites have been identified in GPCRs by X-ray crystallography and recently also cryoelectron microscopy (cryo-EM).[9] For many receptors binding poses of several different types of ligands have been resolved.[10–12] These ligand binding sites have been localized basically anywhere in the receptor structures in agreement with the notion that GPCR ligands do not function by binding to a particular trigger region but rather act as agonists and inverse agonists/antagonists merely by stabilizing active and inactive receptor conformations, respectively.[13–15] Nevertheless, most binding sites for both natural and small synthetic agonists and antagonists are located at the bottom of the extracellular vestibule (ECV). Importantly, after the initial celebrations of obtaining these fascinating, elusive structures, the sobering conclusion has been that the static structures explain surprisingly little about differences in basic pharmacological properties, such as ligand affinities,

association and dissociation rates, receptor/ligand selectivity, etc.[16] Thus, it has become increasingly clear that such pharmacological properties are often determined by dynamic ligand-receptor interactions occurring along the binding path toward the often rather deeply located orthosteric binding sites as demonstrated by molecular dynamic (MD) simulations.

MD simulations were first applied to GPCRs a decade ago,[17,18] and recently they have revealed the dynamic and structural basis, e.g., allosteric modulation and the existence of metastable binding sites and cryptic binding pockets.[19–21] Using advanced computational methods, it has, for example, been demonstrated that receptor selectivity can be determined by differences in the entry path of the ligand, although there were no significant variances in the orthosteric binding pockets of the receptors.[22,23]

For SUCNR1, two high-resolution X-ray structures have been published, i.e., a humanized rat SUCNR1 in complex with the human-selective antagonist NF-56-EJ40 (PDB: 6rnk) and a—for GPCRs—unique apo-structure of the surprisingly stable rat SUCNR1 (PDB: 6ibb).[24] The antagonist, NF-56-EJ40, is bound in a "vertical" pose with its carboxylate head group interacting with two arginine residues located deep between TM-III and -VII.[24] Based on molecular modeling and receptor mutagenesis, these arginines had already, when SUCNR1/GPR91 was deorphanized, been proposed to be the orthosteric binding site for succinate, which recently was confirmed.[2,25–27] Succinate only consists of two carboxylate moieties connected by a simple two-atom hydrocarbon linker and is accordingly expected to bind and activate SUCNR1 almost exclusively through charge-charge and H-bond interaction.[26] No structural information is available concerning succinate binding to SUCNR1; however, recent studies of various SUCNR1 agonists indicate that succinate activates SUCNR1 in its *cis* conformation.[25,26]

Here, we study the binding of succinate and *cis*-epoxy succinate (CES) to SUCNR1 by use of both unbiased MD simulations and metadynamics simulations combined with receptor mutagenesis. Surprisingly, we identify a second high-affinity succinate binding site located high up in the ECV. Here, two arginines in TM-VI serve both as a temporary binding site for succinate on its way down to the orthosteric site but, importantly, also as a real binding site allowing for the unexpected simultaneous binding of two succinate molecules. We propose that this dual binding mode is the molecular basis for the selective activation mechanism of the receptor by high local concentrations of succinate. Moreover, the simulations demonstrate that succinate binding directly unlocks the constrained extracellular loop (ECL)-2b. Interestingly, the antagonist NF-56-EJ40 enters SUCNR1 through another path where non-conserved "gating" residues in TM-I appear to explain its species selectivity.

RESULTS

To understand ligand binding to SUCNR1, we employed all-atom unsupervised MD simulations as well as well-tempered metadynamics simulations combined with receptor mutagenesis. We mainly studied the binding of the endogenous agonist succinate (43 simulations, 90 μs total, Table S1; plus 13 simulations, 15 μs total performed with extra NaCl, see below, Table S3) but also CES (Figure S2A) in which the two carboxylates are confined to *cis* conformation by an epoxy ring (11 simulations 37.1 μs total, Table S2). The binding mode and events were in all respects very similar for succinate and CES, which is therefore not specifically mentioned in the following. As receptor targets, we primarily used the high-resolution humanized rat SUCNR1 structure (PDB: 6rnk); however, when examining the increased flexibility of ECL-2b induced by ligand binding, we also use the rat SUCNR1 apoprotein structure (PDB: 6ibb) (Tables S1–S3) for comparison (see below). For the unsupervised MD simulations, 10 agonists in their fully deprotonated form were placed randomly in the solute at least 15 Å from the extracellular part of the receptor molecules. The ligands were allowed to move freely to find and interact with the receptor both extra- and intracellularly in accordance with the physiological conditions with high succinate concentrations both intra- and extracellularly during metabolic stress. In all 67 simulations, succinate or CES spontaneously bound to the ECV site within an average of 300 ns (Tables S1 and S2), conceivably due to the strong electrostatic attraction of the anionic ligand by the many positively charged residues in the ECV of SUCNR1.

The binding of succinate is guided by a network of arginines

A unique network of five conserved arginines is important in both attracting, guiding, and binding the small dicarboxylate succinate ligand (Figure 1A). Three of these arginines R255$^{6.62}$, R251$^{6.58}$, and R248$^{6.55}$ are positioned on consecutive helical turns down along the extracellular segment of TM-VI stretching from R255$^{6.62}$ at the outer rim of the ECV down to R248$^{6.55}$, which forms the deep orthosteric succinate binding site together with R276$^{7.39}$ from TM-VII and R95$^{3.29}$ from TM-III (Figure 1A). In the simulations where succinate reaches this deep orthosteric binding site, it interacts consecutively with all members of the arginine network through both charge-charge interactions as well as close H-bond and water-mediated interactions (Figures 1B–1D). In all 54 simulations, succinate initially binds between the outermost R251$^{6.58}$ and R255$^{6.62}$ and in 33 cases just stays bound in this site for the rest of these MD simulations (Figure 1D). However, in the remaining 21 simulations, succinate is carried down to the deep orthosteric site by a rotation of the side chain of R251$^{6.58}$ (Figure 1B, middle). Thus, located in the middle of the arginine network, R251$^{6.58}$ plays a particularly crucial role in both the initial binding and in the movement of succinate into its final binding site.

The binding of succinate to the orthosteric site happens in three well-defined stages

In the 21 cases where succinate moved down to the orthosteric site, this happened in three well-defined stages as illustrated by the clear stepwise decrease in the distance between the ligand and the bottom of the orthosteric pocket (Figure 1B.). Stage 1, where succinate is bound in the ECV site (Figures 1B and 1C, blue), is followed by an intermediate stage (Figures 1B and 1C, red) and stage 2, corresponding to the final binding in the deep orthosteric site (Figures 1B and 1C, green). In most simulations with the humanized rat SUCNR1, succinate initially interacts with K266$^{7.29}$ and N269$^{7.32}$ at the exterior pole of TM-VII

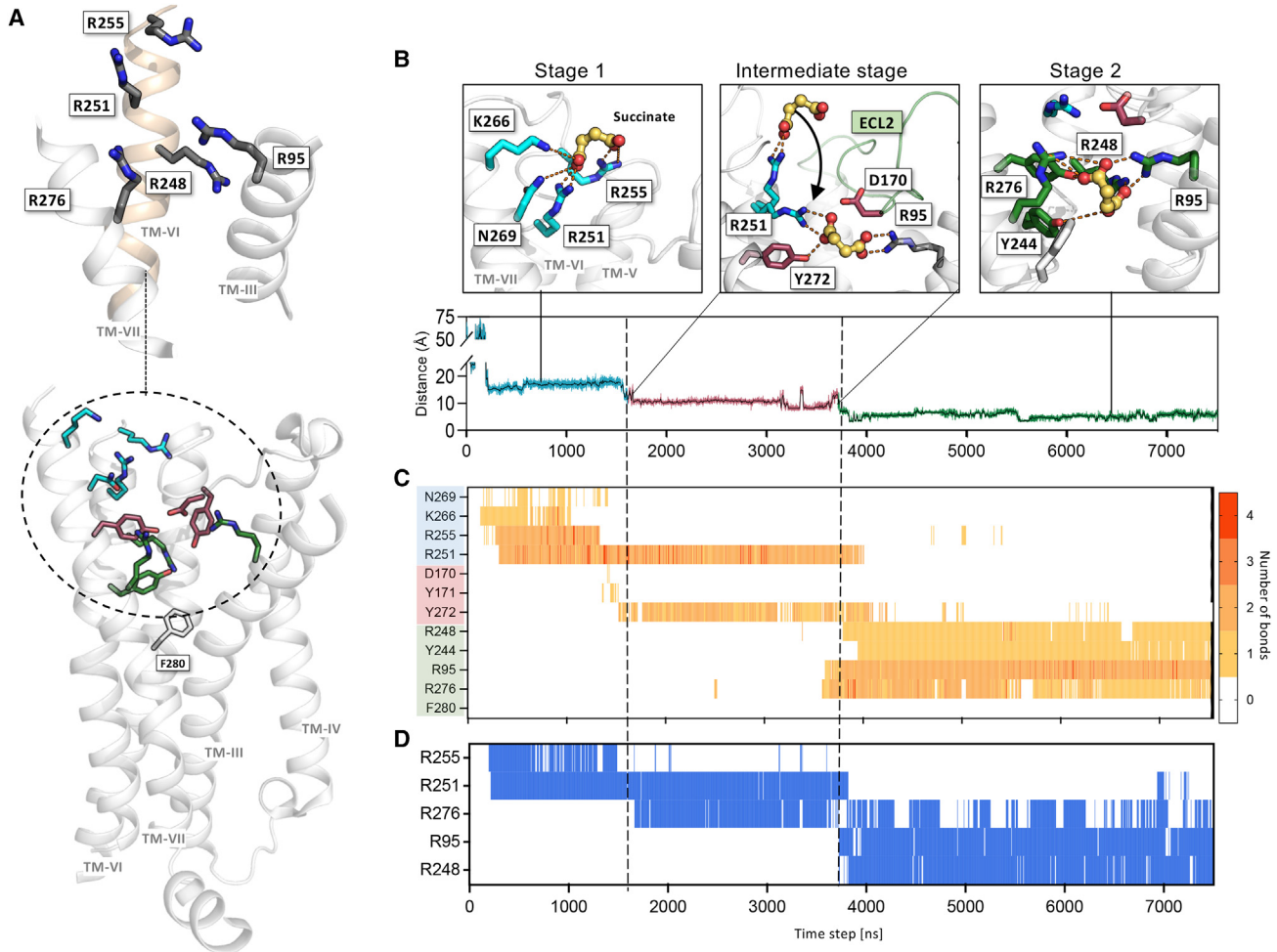

Figure 1. Pathway and dynamics for succinate binding in SUCNR1 during unbiased MD simulations

(A) In the lower fragment are shown residues that succinate interacts with, from its initial binding in the extracellular vestibule in stage 1 (residues highlighted in blue) through the intermediate stage (red residues) to its final binding in the "deep orthosteric site" in stage 2 (green residues), all represented in the crystal structure of the humanized ratSUCNR1 (PDB: 6rnk). F280 is used as a measuring point at the bottom of the orthosteric pocket and is highlighted in white sticks. The top fragment focuses on the special network of five arginines around the inner face of the extracellular segment of TM-VI (in light brown) of SUCNR1, of which R255$^{6.62}$ and R251$^{6.58}$ in TM-VI form the initial catching ECV site and R248$^{6.55}$ together with R95$^{3.29}$ and R276$^{7.39}$ form the main components of the deep orthosteric site.

(B) Distance between the center of the mass of succinate and the bottom of the orthosteric pocket (center of masses of F280) throughout MD simulation ID: 33 (Table S1) with the three stages highlighted in blue, red, and green. The left insert top (stage 1) shows succinate initially caught by K266$^{7.29}$ and N269$^{7.32}$ and firmly bound between R255$^{6.62}$ and R251$^{6.58}$ in TM-VI. Middle insert top (intermediate stage)—R251$^{6.58}$ is shown in two rotational conformations, illustrating how in the intermediate stage it carries the tightly bound succinate down from the ECV site to pass between D170$^{45.52}$ in ECL-2b and Y272$^{7.35}$ (see Figure 4 concerning water-mediated breakage of H-bond). Right, insert top (stage 2)—succinate bound between R95$^{3.29}$, R248$^{6.55}$, R276$^{7.39}$, and Y272$^{7.35}$.

(C) Heatmap of the number of direct and water-mediated H-bond interactions between succinate and residues in SUCNR1 throughout the MD simulation (ID #33)—with the time point of the three binding stages indicated by vertical dotted lines.

(D) Long-range charge-charge interactions (atomic distance <5 Å) between succinate and each of the five arginines during the MD simulation (ID: 33). In stage 1, succinate is bound between the upward-turned R251$^{6.58}$ and R255$^{6.62}$, in the intermediate stage, interacting with the downward-turned R251$^{6.58}$ and R276$^{7.39}$, and in stage 2, it is bound between R276$^{7.39}$, R95$^{3.29}$, and R248$^{6.55}$ in the deep orthosteric site.

before becoming sandwiched between R255$^{6.62}$ and R251$^{6.58}$ (Figures 1B–1D). The crucial role of R251$^{6.58}$ as a key interaction partner for succinate not only in stage 1 but also during the entire intermediate stage is illustrated by the two heatmaps of ligand-receptor interactions (Figures 1C and 1D). The abrupt shift from stage 1 to the intermediate stage (Figure 1B) is preceded by a loss of the interaction between succinate and R255$^{6.62}$, which allows for the subsequent approximately 6 Å downward transfer of the succinate molecule. This transfer is mediated through a rotation of the R251$^{6.58}$ side chain around its χ_1 bond with succinate closely bound to its terminal guanidyl moiety (Figure 1B, middle). The final downward movement of succinate to the orthosteric site (stage 3), occurs when it forms an H-bond with R276$^{7.39}$ in TM-VII and R95$^{3.29}$ in TM-III

(Figures 1C and 1D). In fact, succinate continues to interact intermittently with R251$^{6.58}$ until it finally settles closely sandwiched in its *cis* conformation between R95$^{3.29}$, R248$^{6.55}$, and R276$^{7.39}$ and with Y244$^{6.51}$, its fourth interaction partner which forms the base of the deep orthosteric site (Figures 1C and 1D). Very similar binding dynamics of succinate in respect of stage-wise binding and interaction with key residues was observed when extra Na+ and Cl− ions (33 atoms of each) were included in the aqueous phase to mimic a physiological NaCl concentration of 0.15 M (Figure S3; Table S4).To further validate this, we performed additional 13 simulations with total simulation time of 15 μs. (Table S4; Figure S6)

Throughout the binding process, succinate is found in its preferred *cis* conformation even more than observed in the unbound water interacting state (Figure S2B). However, in the intermediate stage, succinate changes more frequently to its *trans* conformation than in stage 1 and stage 2, reflecting the interchange between different binding poses in the intermediate stage (Figure S2B). Nevertheless, even in the intermediate stage, succinate is still only in its *trans* conformation a small percentage of the time, which agrees with the fact that CES in all respects behaves very similar to succinate in the MD simulations.

There are two low-energy succinate binding sites in SUCNR1

To study the free-energy profile of the succinate ligand binding path, we employed well-tempered metadynamics simulations where a single succinate molecule was placed in a random position and orientation above the extracellular surface of the receptor at a distance of at least 15 Å. We used the center of masses of the ligand and F280 at the bottom of the orthosteric pocket as a collective variable (CV). These metadynamics simulations consistently demonstrated the existence of two energy minima (Figure 2B, blue and green circle) corresponding to succinate binding in the ECV site and the orthosteric pocket, respectively (Figure 2A, green and blue pocket). Interestingly, between these two binding modes, an energy barrier was observed which the ligand must overcome to transition from the ECV to the orthosteric site as observed in 21 of the 54 unbiased MD simulations. We speculate that the high energy of the intermediate stage is related to the conformational changes occurring in the receptor (see below).

To explore the effect of these key residues, we performed single-point mutations in both the human and mouse SUCNR1. In them, we mutated both the ECV and orthosteric binding pocket. Our results are consistent with the simulations and show that although the human receptor differs with respect to the most exterior K269$^{7.32}$ being replaced with an asparagine residue, the rat and mouse receptors are identical concerning all residues of the succinate binding path (Figure S1). Several residues of the orthosteric binding site have been mutated previously,[2,25,26] and, as expected, we observed that substitutions of R95$^{3.29}$, R248$^{6.55}$, and R276$^{7.39}$ in both mouse and human SUCNR1 all seriously affected or even eliminated succinate ability to activate the receptors (Figures S7A, S7B, S8A, and S8B). Interestingly, substitutions of the charged residues in the ECV site shifted the dose-response curve for succinate activation of SUCNR1 to the right (Figure 2C). Significantly, alanine substitution of R251$^{6.58}$ and R255$^{6.62}$ both impaired succinates potency in SUCNR1 activation more than 100- or 1,000-fold. Indicating that, although they are in the ECV site far above the orthosteric binding site, these residues in the binding, entry path are also crucial for the ability of succinate to activate SUCNR1 (Figures 2C, S7, and S8).

Further, we made double and triple mutants to systematically probe the importance of the Args in the ECV and try and remove the ECV binding pocket all together for both mouse and human SUCNR1 (Figures S7I, S8I, and S9C). Mutation K266$^{7.29}$A K269$^{7.32}$A resulted in significant decrease of both potency and efficacy, but receptor signaling was still registered. On the other hand, mutations including an Arg—R255$^{6.58}$A K266$^{7.29}$ and triple mutant R255$^{6.58}$ K266$^{7.29}$A K269$^{7.32}$A resulted in complete loss of signal, underlining the importance of the ECV binding site for the overall mechanism of receptor activation.

Two succinate molecules can bind simultaneously to SUCNR1

In 17 of the 54 unbiased MD simulations, we surprisingly observed simultaneous binding of two succinates (or two CES) molecules, i.e., with one binding in the orthosteric site and another in the ECV site (Tables S1, S2, and S4). Interestingly, this dual ligand binding happened in two very different ways, i.e., a sequential or a "bypass" binding mode (Figures 2D and 2E). Sequential binding of a second succinate occurred in six of the 21 cases where the "first" succinate had moved down from the ECV site to the deep orthosteric site, and the second succinate subsequently bound to the vacant ECV site (Figure 2D; Tables S1 and S2). More surprisingly, in 11 out of the 17 cases where the first succinate molecule stayed bound to the ECV site, a second succinate bypassed the first succinate to access and bind to the orthosteric site (Figure 2E; Table S1, S2, and S4). This bypass binding of a second succinate occurred in a single uninterrupted stage, conceivably attracted by the electrostatic potential of the three unoccupied arginines of the orthosteric site where the succinate made close H-bond interactions initially with R276$^{7.39}$ rapidly followed by R95$^{3.29}$ and R248$^{6.55}$ (Figures S5A, S5B, and S6). During its downward movement, the second succinate only made a few, short-lived H-bond interactions with R251$^{6.58}$ while passing the first succinate, which was bound to and neutralized the electrostatic potential of R255$^{6.62}$ and R251$^{6.58}$.

Interestingly, in all six cases of the sequential mode, where the second succinate bound to the vacated ECV site, it surprisingly unbound after 200–1,200 ns (Tables S1, S2, and S4), indicating that the partial neutralization of the electrostatic potential of the three arginines of the deep orthosteric site by the binding of the first succinate destabilizes the ECV site (Figures 2D and S5A). Nevertheless, in only one of the 11 cases of "bypass binding" did the first, ECV-bound succinate leave the receptor again (#7 in Table S1).

Species-selective binding of antagonist is determined mainly by its distinct entry path

NF-56-EJ40 is a potent, highly human-selective SUCNR1 antagonist, which was co-crystalized with the humanized rat SUCNR1, in which N18$^{1.31}$ in TM-I and K269$^{7.32}$ in TM-VII both located at the outer rim of the ECV were substituted with E and

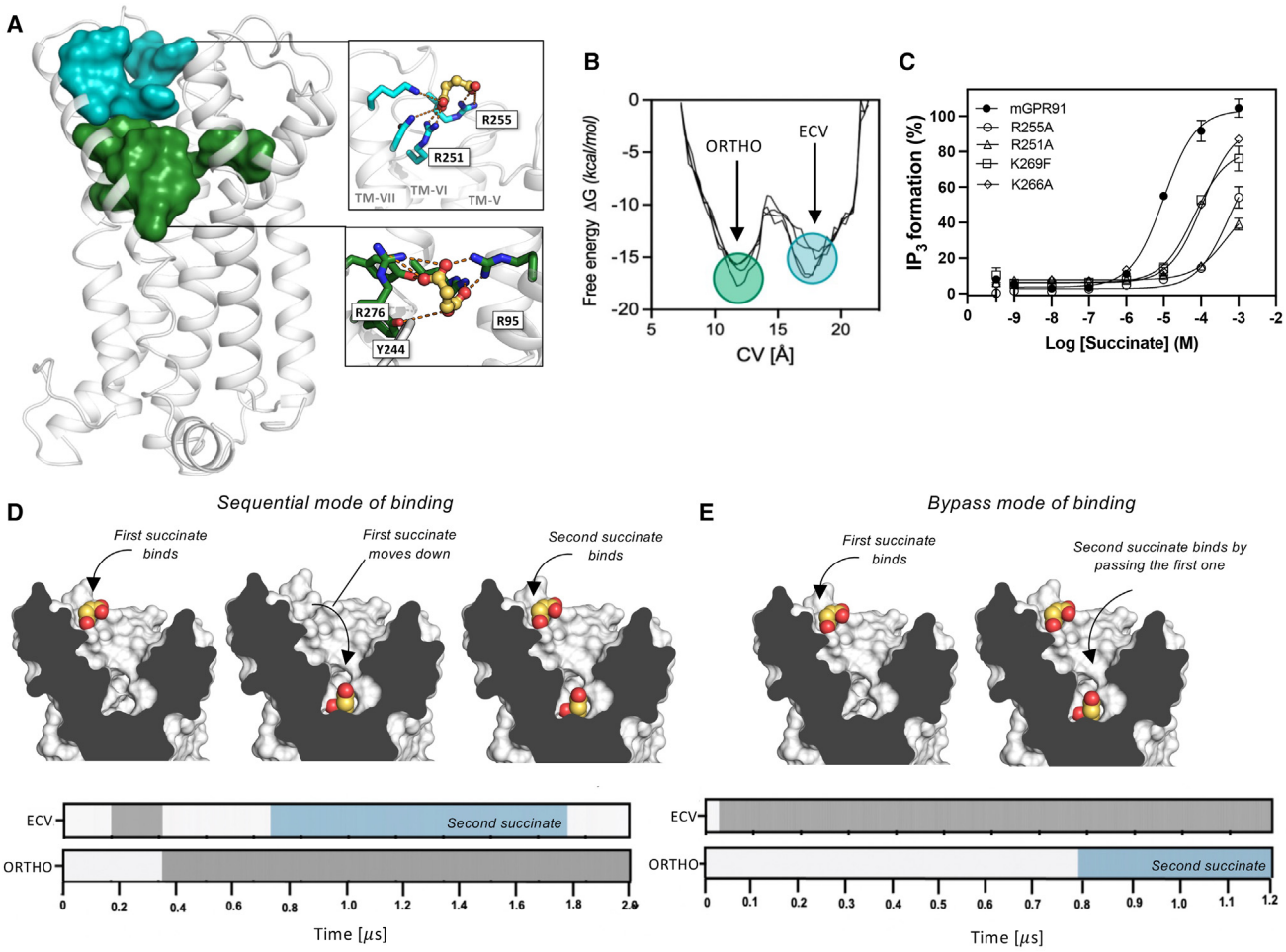

Figure 2. The two low-energy succinate binding sites in SUCNR1 and how they can get simultaneously occupied by two succinate ligands

(A) The two binding sites for succinate represented as surface in the humanized ratSUCNR1 (PDB: 6rnk): in blue, the ECV site between the outer poles of TM-VI and TM-VII indicated in the corresponding insert to the right; in green the deeper, orthosteric site between TM-III, TM-VI, and TM-VII indicated in the corresponding insert to the right.

(B) Well-tempered metadynamics analysis of succinate binding to SUCNR1 revealing two energy minima corresponding to binding to the ECV site (blue circle) and orthosteric site (green circle), respectively. The intermediate binding state between the two low-energy binding modes is associated with an energy barrier, which must be overcome when the ligand passes from the ECV site (stage 1) to the orthosteric binding site (stage 2). Four replicates are shown, and the collective variable (CV) is the distance between the center of the masses of succinate and F280.

(C) Mutational analysis of the ECV binding site in murine SUCNR1 using activation of Gq-mediated IP3 accumulations in transfected COS7 cells as a functional readout for the R251$^{6.58}$A, R255$^{6.62}$A, K266$^{7.29}$A, and K269$^{7.32}$A mutants versus WT murine SUCNR1 (n = 3, error bars represented as ± SEM). A similar mutational analysis of the orthosteric site is shown in Figures S5 and S6.

(D) Simultaneous binding of two succinate molecules through a sequential mechanism. The first ligand molecule binds in the ECV site and then moves down to the orthosteric site through the stepwise mechanism described in Figure 1—this happens in 21 of the 54 unbiased MD simulations performed with either succinate or CES (Tables S1 and S2). A second succinate binds in the vacant ECV site while the first occupies the orthosteric site, which happens in six of the 21 cases; however, the second succinate in all six cases left the ECV site again before the end of the MD simulation. The occupancy plot below shows the timeline for each of the two sites with the first succinate indicated in gray and the second succinate indicated in blue for MD #27.

(E) Simultaneous binding of two succinate molecules through the bypassing mechanism. The first succinate stays bound in the ECV site between R251$^{6.58}$ and R255$^{6.62}$, while a second succinate molecule bypasses the first succinate to get directly bound in the triple-arginine orthosteric deep site. The occupancy plot below shows the timeline for each of the two sites for MD #2. Occupancy timeline plots for all MD simulations where dual succinate occupancy was observed using PDB: 6rnk are shown in Figure S5.

N, respectively (PDB: 6rnk).[24] To understand the binding and molecular mechanism of action of NF-56-EJ40 in more detail, we used well-tempered metadynamics simulations in which we used the distance between the center of the masses of the ligand and F280 at the bottom of the orthosteric pocket as CV. The energy landscape for the antagonist binding displayed a single low-energy minimum corresponding to the final binding pose with only a minor shoulder corresponding to the entry phase (Figure 3A). The mono-carboxylate antagonist initially, intermittently interacted with positively charged residues of the ECV succinate

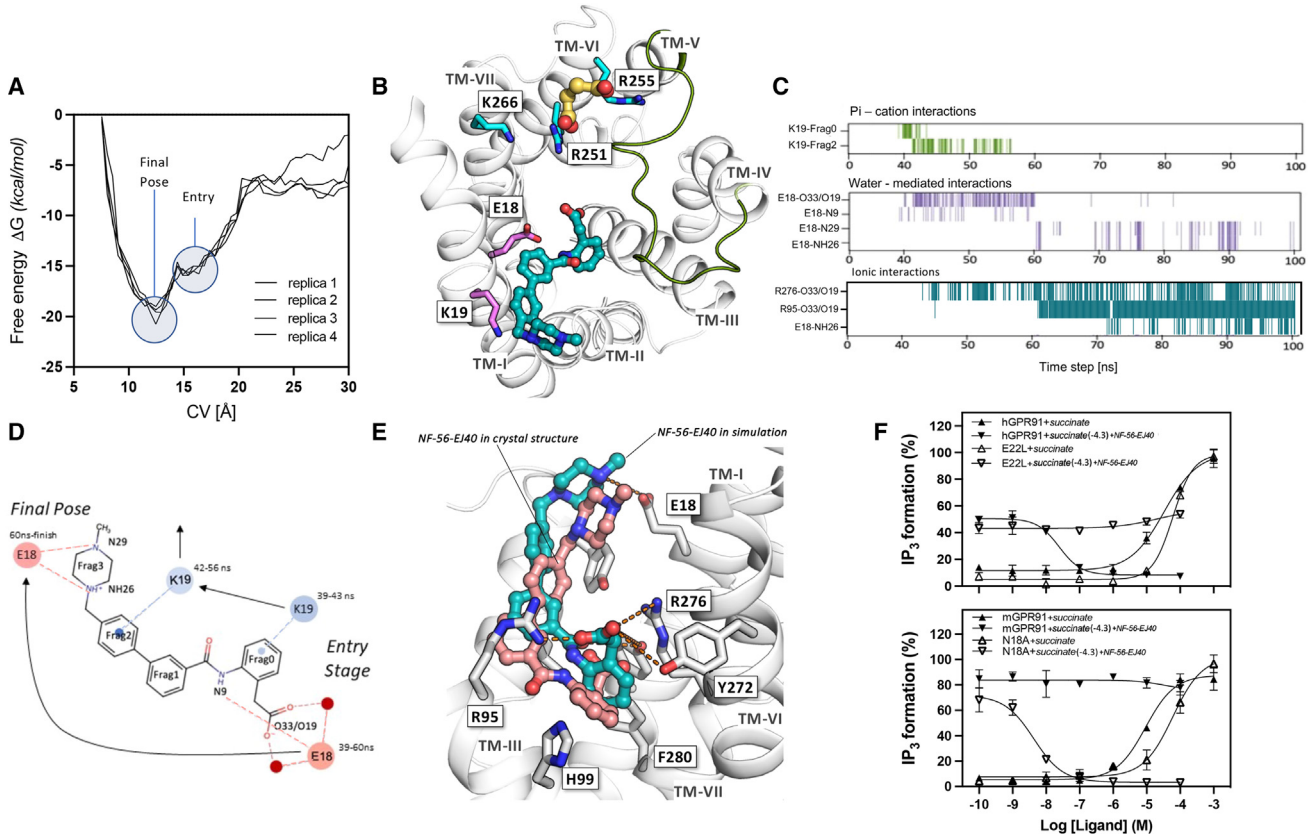

Figure 3. Molecular dynamics simulations of antagonist NF-56-EJ40 binding to SUCNR1

(A) Free-energy landscape of NF-56-EJ40 binding to SUCNR1 (PDB: 6rnk) obtained from well-tempered metadynamics. CV, the distance between the center of masses of the antagonist and F280 (see STAR Methods for details). In all four representative experiments, the free-energy landscape demonstrates that binding occurred in a single stage with only a "shoulder" corresponding to the entry phase.

(B) Top view of the entry poses of NF-56-EJ40 between TM-I and TM-II in close contact with E18$^{1.31}$ and K19$^{1.32}$. For comparison, a succinate molecule is shown in its very different entry position between TM-VI and -VII (see Figures 1 and 2).

(C and D) Different types of molecular interactions between NF-56-EJ40 and key SUCNR1 residues during the binding process are shown in a heatmap format in (C) and in schematic form for E18$^{1.31}$ and K19$^{1.32}$ in (D). K19$^{1.32}$ forms cation-p interactions with two of the aromatic rings during the entry phase for the antagonist. First, E18$^{1.31}$ makes water-bridged H-bond interaction with the head group carboxylate, as well as with the amide linker of the antagonist and eventually shifts to making both water-mediated and ionic interactions with the terminal piperazine moiety in the final bound pose. R276$^{7.39}$ and R95$^{3.29}$ of the orthosteric succinate binding sites make ionic interactions with the head group carboxylate of the antagonist.

(E) Superimposition of a representative frame of the bound NF-56-EJ40 from the metadynamics simulations (blue) and the structure of NF-56-EJ40 with SUCNR1 (PDB: 6rnk) (pink).

(F) Mutational analysis of 1.31 in the entry path for NF-56-EJ40. The top shows loss of function with respect to antagonist action in the human SUCNR1, i.e., E22$^{1.31}$L mutation, which is involved in both antagonist entry and in stabilizing the final pose of the antagonist (n = 3, error bars are represented as ± SEM) (E). The bottom shows the gain of function of the antagonist action in the murine SUCNR1 mediated by N18A$^{1.31}$ substitution, which in the wild-type murine SUCNR1 prevents entry and function of the antagonist. In both cases, the mutants have only minimal effect on the succinate activation of the receptor.

binding site at the top of TM-VI and -VII (Figures S4C and S4D) after which it surprisingly entered the ECV between TM-I and -II with its the carboxylate (Figure 3B). The primary real interaction partners for the antagonist were K19$^{1.32}$ pointing toward TM-II and the mutationally introduced E18$^{1.31}$ pointing toward the center of the receptor (Figures 3B and S7J). The initial strong interaction was a close cation-p interaction between the e-amino group of K19$^{1.32}$ and the benzyl ring entitled Frag0 of the antagonist, whereas E18$^{1.31}$ surprisingly interacted with the carboxylate spearhead moiety of the antagonist through water-mediated H-bonds and the amide nitrogen (N9) located on the other side of Frag 0 of the ligand (Figures 3C and 3D). As the antagonist moved in, K19$^{1.32}$ shifted from Frag0 to instead making close, cation-p interactions with the Frag2 benzyl group, whereas the spearhead carboxylate established ionic interactions with R276$^{7.39}$ of the deep orthosteric succinate site but still interacted with E18$^{1.31}$ through the water-mediated H-bonds (Figures 3C and 3D). As the antagonist moved further in and downward to interact strongly also with R95$^{3.29}$ of the deep orthosteric site, the ligand lost contact with K19$^{1.32}$, whereas E18$^{1.31}$ shifted from interacting with the leading carboxylate to interacting with the nitrogen atoms of the piperazine ring at the other end of the antagonist molecule (Figures 3C and 3D). As shown in Figure 3E, the final, stably bound pose of the antagonist in our

simulations was superimposed on the antagonist-bound crystal structure. The two binding modes were in good agreement.

Because our MD simulations indicated that E18$^{1.31}$—originating from in the human SUCNR1—together with the critical, conserved K19$^{1.32}$ plays a positive role in the entry phase of the antagonist (Figures 3B–3D), we hypothesized that the inability of NF-56-EJ40 to bind to mouse SUCNR1 could be due to the inability of the corresponding asparagine in position 18 of the murine receptor to assist ligand entry and that the asparagine residue instead potentially could inhibit antagonist binding. Thus, we performed metadynamics simulations similarly as previously described with the humanized SUCNR1 with either asparagine or alanine residue at position 18. In the metadynamics simulations with N18$^{1.31}$, we did not—as expected—observe any binding of NF-56-EJ40, whereas in simulations with Ala in position 18, we observed NF-56-EJ40 binding where the antagonist entered between TM-I and -II while making cation-p interactions with K19$^{1.32}$ and with a final binding pose with its spearhead carboxylate binding to the arginines of the orthosteric site similar to that in the humanized receptor as previously observed (Figure S7).

Importantly, in the signal transduction assays, the substitution of E18$^{1.31}$ in the human receptor with a large aliphatic leucine residue—as expected—eliminated the ability of NF-56-EJ40 to antagonize succinate-stimulated signaling (Figure 3F, upper). As expected, in the wild-type (WT) murine SUCNR1 no effect was observed with NF-56-EJ40, whereas "removal" of the N18$^{1.31}$ side chain with an alanine made the otherwise inactive NF-56-EJ40 an efficacious and surprisingly potent antagonist of succinate-induced signaling (Figure 3F, lower). Thus, the N18$^{1.31}$ to Ala mutation demonstrates that NF-56-EJ40 can bind and both potently and efficiently antagonize SUCNR1 without a glutamic acid in position 18, which otherwise was believed to be essential for its binding.[24]

Our simulations demonstrate that NF-56-EJ40 enters SUCNR1 between the extracellular ends of TM-I and -II and that, although the Lys in position 19 in TM-I is the key interaction partner, the residue at position 18 determines the species selectivity of the antagonist mainly due to its role in ligand entry rather than its role in the final pose of the antagonist.

Agonist, but not antagonist, entry unlocks ECL-2b conformational constraint

In all SUCNR1 crystal structures (PDB: 6ibb, 6rnk, and 6z10),[24,28] ECL-2b has a characteristic hairpin-like conformation, reaching relatively deep into the ECV as observed also in the closely related P2Y1 structure.[29] In both receptors ECL-2b is held in this constrained conformation by an aspartic acid residue, D170$^{45.52}$ in SUCNR1, making an H-bond to Y272$^{7.35}$ in TM-VII. (Figure 4A, left). D170$^{45.52}$ is in two positions after C168, which separates ECL-2 into the a and b parts through the conserved disulfide bridge to a Cys residue at the top of TM-III (Figures 4B and 4C).

In the MD simulations, the distance between D170$^{45.52}$ and Y272$^{7.35}$ remained short—i.e., approximately 3.2 Å—and very stable during stage 1 while succinate is still bound in the ECV binding site (Figure 4A). However, in the early part of the intermediate stage, i.e., when the R251$^{6.58}$-bound succinate molecule passes close by these residues on its way down toward the deep orthosteric site, the H-bond between D170$^{45.52}$ and Y272$^{7.35}$ breaks and the distance between these residues increased to 6–8 Å for the rest of the MD simulations (Figure 4A). Breakage of the H-bond results in a major movement of ECL-2b away from TM-VII (Figure 4B). This is associated with increased flexibility of the residues surrounding D170$^{45.52}$ as quantified by increases of their RMSF values in systems with succinate or CES prebound compared with the apo-form of the receptor and or NF-56-EJ40 prebound (Figure 4D; Table S3). Breakage of the H-bond between D170$^{45.52}$ and Y272$^{7.35}$ occurred in all 32 cases where succinate passed down either as the first agonist—21 cases—or as the second by the bypass mechanism—11 cases (Tables S1, S2, and S4).

Based on the observation that interactions between succinate and D170$^{45.52}$ almost exclusively were water mediated, whereas its interactions with, e.g., R251$^{6.58}$, are through direct H-bonds (Figures 1D and 4E), we performed a deeper analysis of the movements of the water molecules relative to each other and to residues in the agonist binding path during the simulations. Here, we observed the formation of two well-defined clusters of water molecules during the intermediate stage of succinate binding. Initially, water cluster "A" formed between the two carboxylic moieties of the R251$^{6.58}$-bound succinate molecule—in *cis* conformation—and D170$^{45.52}$ and Y272$^{7.35}$ as it passed by these residues but decreased in size and disappeared when the distance between these residues increased due to the breakage of the H-bond between them (Figure 4F). A second, larger water cluster B formed close to cluster A between the downward rotated R251$^{6.58}$ and D170$^{45.52}$, as well as R248$^{6.55}$ (Figure 4F). Unlike cluster A, cluster B decreases more slowly in size and first disappeared when succinate was firmly bound to the orthosteric site and R251$^{6.58}$ rotated back up.

Importantly, binding of the NF-56-EJ40 antagonist, which after its entry between TM-I and -II subsequently moves down between TM-II and -VII to bind in the same deep orthosteric site, in no cases resulted in breakage of the ECL-2b stabilizing H-bond as also reflected in the lack of increase in RMSF values for D170$^{45.52}$ and its surrounding residues in ECL-2b (Figure 4D). This is probably because the antagonist in contrast to succinate only has a single carboxylate moiety and consequently cannot contribute as much to the formation of a water cluster and that it does not get close enough to D170$^{45.52}$ and Y272$^{7.35}$. Mutations of D170$^{45.52}$A did not significantly affect the receptor signaling in inositol phosphate (IP) accumulation (Gq-pathway) and cyclic AMP (cAMP) inhibition (Gi-pathway) for both mouse and human (Figures S7E, S7F, S8E, and S8F). Mutations of Y272$^{7.35}$A resulted in loss of receptor signaling because Y272$^{7.35}$ is part of the succinate binding orthosteric pocket (Figures S7I, S8I, and S9C).

It is concluded that the close passage of the two carboxylates of succinate in their *cis* conformation and the formation of a water cluster between them and D170$^{45.52}$ and Y272$^{7.35}$ destabilizes the H-bond between these two residues and thereby liberates ECL-2b from its locked position (Figure 4B), which we propose could be part of the receptor activation mechanism.

DISCUSSION

By use of both unsupervised MD and metadynamics simulations, we here identify how a unique motif of five-arginine

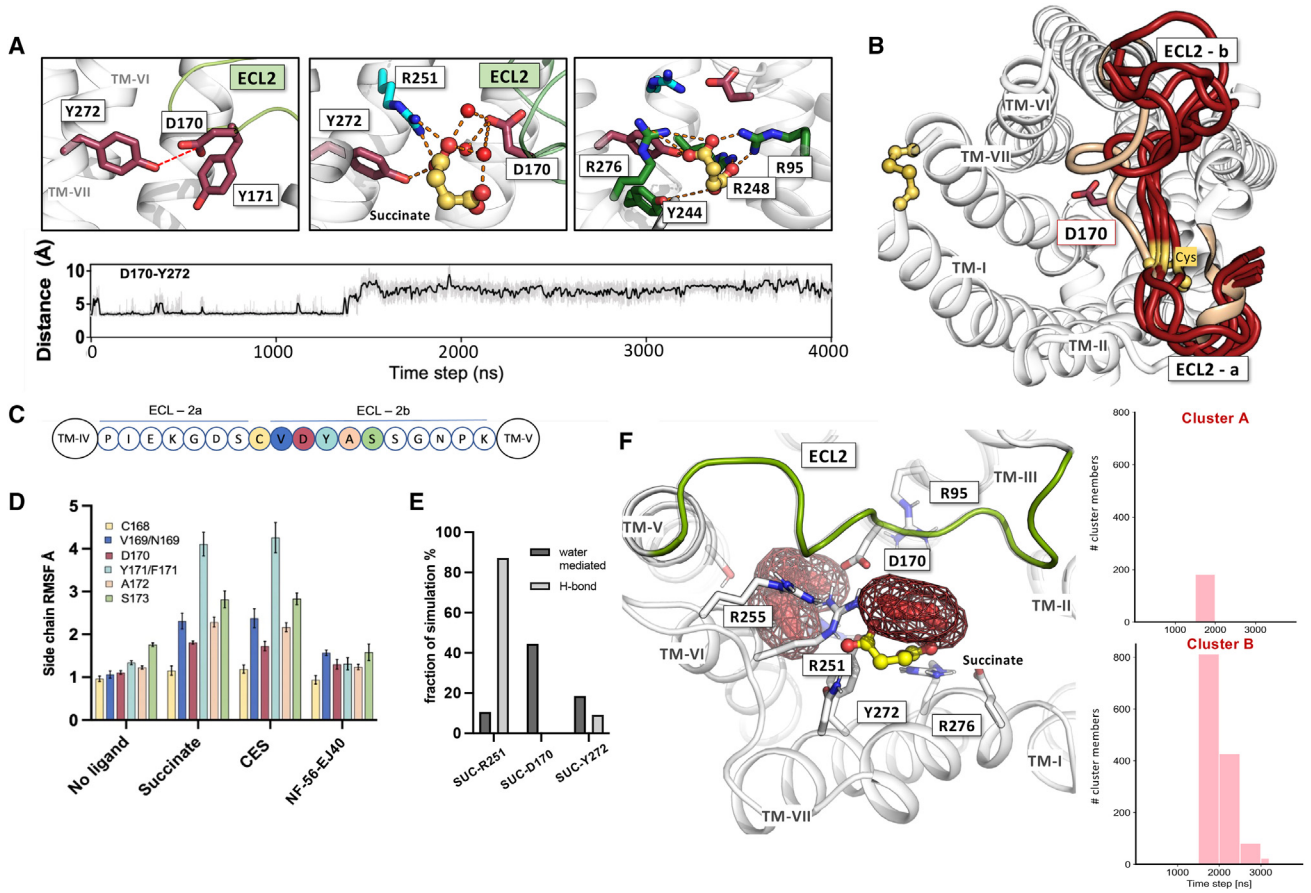

Figure 4. Breakage of constraining H-bond and conformational changes induced in ECL-2b of SUCNR1 by succinate (agonist) passage and water cluster formation

(A) The distance between the carboxylate Cα of D170$^{45.52}$ and Cα of Y272$^{7.35}$ throughout MD simulation of SUCNR1 (ID #20, Table S1). Left panel top, a snapshot of Y272$^{7.35}$ and D170$^{45.52}$ in stage 1, where the H-bond between these residues is highly stable. Middle top, snapshot from the intermediate stage where succinate in its *cis* conformation is passing, the H-bond is broken and D170$^{45.52}$ with ECL-2b has moved away. In this frame, water molecules make H-bond bridges between the succinate carboxylates and D170$^{45.52}$. Right top, stage 2 where succinate has moved down into the orthosteric site but D170$^{45.52}$ and Y272$^{7.35}$ stay apart as ECL-2b remains open.

(B) Top view of SUCNR1 shows the conformational change of ECL2 upon agonist binding through the trajectory (from wheat to red).

(C) Sequence of SUCNR1 ECL2 divided into 2a and 2b by the conserved Cys with D170$^{45.52}$ highlighted in red and surrounding residues highlighted in different colors.

(D) Root mean square fluctuations (RMSFs) of the side chains of the first residues of ECL-2b in SUCNR1 in the apo forms (PDB: 6ibb), with succinate, CES, or antagonist bound. The bars average four replicas per setup (Table S3).

(E) H-bond versus water-mediated interactions between succinate and R251$^{6.58}$, D170$^{45.52}$, and Y272$^{7.35}$ during the MD simulation demonstrating that succinate interacts exclusively via water molecules with D170$^{45.52}$ and to a large degree with Y272$^{7.35}$ as opposed to R251$^{6.58}$.

(F) Formation of clusters of water molecules around succinate, D170$^{45.52}$, Y272$^{7.35}$, and R251$^{6.58}$ during the intermediate stage of succinate binding—top view of SUCNR1. Cluster A is formed between succinate in its *cis* conformation and D170$^{45.52}$ and Y272$^{7.35}$ and disappears with the increase of distance between these residues. Cluster B is formed between the downward bend R251$^{6.58}$, D170$^{45.52}$, and R248$^{6.55}$ and gradually decreases in size as the succinate molecule reaches its final bound pose and R251$^{6.58}$ swings upward.

residues around the extracellular pole of TM6 defines how SUCNR1 captures succinate to either stay bound in the ECV site between the two exterior arginines or move down to eventually bind between the three lower arginines of the deep orthosteric site. Importantly, the MD simulations demonstrate that SUCNR1 activation most likely is dependent upon the concomitant binding of two succinate molecules—one in each site, which we propose explains how SUCNR1 is tuned to be activated by very high, local concentrations of succinate in a highly selective manner.

A second, allosteric succinate binding site in SUCNR1

Based on molecular modeling and mutational analysis, it was already in the original deorphanization study proposed that arginine residues located relatively deep between the diverging extracellular helical segments constituted the orthosteric binding site for the dicarboxylic succinate.[2] This site corresponds to the classical binding sites for small GPCR agonists such as catecholamines, acetylcholine, and histamine.[30] In several of these receptors, binding sites for synthetic allosteric modulators have been identified higher up in the ECV.[20,31] Recently, Burger

et al.[32] reported a new cryo-EM structure M4 mAChR, in which they observed the concomitant orthosteric and allosteric binding of xanomeline, further supporting the notion that there is much more to be uncovered about ligand binding paths and the way they can regulate GPCRs. Although MD simulations have demonstrated that agonists, as part of their entry path, can occupy or bind to such an allosteric site for a short while, these ECV sites have never been shown to function as an additional binding site for the concomitant binding of endogenous agonists—as we here observed for SUCNR1. Thus, our metadynamics simulations clearly demonstrate low-energy binding of succinate in the ECV site between the two arginine residues located in an *i* and *i* + 4 configuration at the extracellular pole of TM6. Importantly, the metadynamics simulations also revealed that a relatively high energy barrier must be overcome for succinate to move down from the ECV binding site to the deep orthosteric site. This is also reflected in the observation that succinate—or CES—in 33 out of the 53 unbiased agonist MD simulations just stayed bound in the ECV site for the duration of the simulations. Thus, the ECV site evidently plays a key role both as an initial interaction or catching site for the anionic succinate during its entry phase but also serves as a low-energy succinate binding site. The importance of the ECV site for succinate activation of SUCNR1 is underlined by the >100-fold effects on the potency of succinate signaling of mutational substitutions of residues in the ECV site located far "above" the deep orthosteric site.

SUCNR1 binds two succinate molecules concomitantly

Similar MD simulation approaches as the one employed here for SUCNR1 have previously been used for other receptors; however, the binding of just a single ligand was a relatively rare event, and binding of two ligands was never reported.[19,22,23,33–35] However, in all of the 54 unbiased MD simulations with SUCNR1, we observed spontaneous binding of succinate or CES and, in 19 cases even concomitant binding of 2 agonist molecules. Conceivably this is due to the strong long-range electrostatic attraction of the highly anionic ligand by the arginine cluster.[36] The dual binding occurred in two different manners either in an unstable sequential manner or in a more frequent and stable, bypassing manner (Figure 2). Surprisingly the stability of succinate binding in the ECV site was different depending on whether this site became occupied by the first or the "second" succinate. That is, succinate bound very stably to the ECV site when it occupied this site as the first succinate, and the second succinate just passed by this to bind in the deep orthosteric site. In fact, in this scenario we never observed the first succinate leaving the ECV site again, just as succinate never was observed to leave in the cases where no second succinate bound. However, when the ECV site instead was occupied by a second succinate after the first one had moved down to the orthosteric site, this second, sequential succinate did not bind stably because it left again in all cases during the simulations. The structural basis for the more stable binding of succinate in the ECV site in the bypassing mode compared with the sequential mode is not entirely clear. Thus, in both scenarios, the attracting electrostatic potential of the three arginines of the orthosteric site is neutralized by a bound succinate, and in both scenarios, ECL-2b is released by the succinate molecule, which moves down to the deep site—as discussed below.

But what happens under physiological circumstances? All of the above relates to MD simulations of long, but still limited, duration relative to the actual agonist binding and receptor activation events. Nevertheless, based on these MD simulations, we propose that, most likely, there are two main physiological endpoints for succinate binding: (1) SUCNR1 is occupied by only a single succinate molecule bound in the deep orthosteric site after having initially been caught in the ECV site, i.e., because sequential binding of second succinate in the ECV site in this scenario appears to be both an infrequent and an unstable event. (2) SUCNR1 is occupied by two succinate molecules—one in each site being bound through the stable bypass mechanism. Because we observed bypass binding of a second succinate in most cases where the first succinate (or CES) remains bound in the ECV site, we assume that this in fact is the predominant mechanism for ligand binding in SUCNR1.

SUCNR1 signals through both Gi, providing, e.g., autocrine inhibition of lipolysis in adipocytes, and through Gq, which is involved in, e.g., paracrine hyper-polarization of M2 macrophages during tissue repair,[5,6] which are activated at different concentrations of agonist (unpublished data). However, the structural basis and potential association with, e.g., one-ECV versus dual binding modes is unclear and far from straightforward to test. This is because the orthosteric site is involved in both binding modes and because the ECV site serves both as part of the entry path in the single succinate binding mode and as a binding site in the dual binding mode. Potentially, the hypothesis could be addressed, e.g., through accelerated MD simulations including different types of G proteins[37,38] and with either one or two succinates bound.

Concerning dual agonist binding in GPCRs in general, highly efficacious homobivalent bitopic synthetic agonists have been described for, e.g., opioid receptors.[39–41] To the best of our knowledge, whether both the agonist epitopes of these synthetic ligands bind at the same time to a single receptor molecule has not been conclusively demonstrated. However, in the long-chain fatty acid (LCFA) receptor, FFAR1/GPR40 high-resolution X-ray crystallography has revealed two distinct binding sites for lipid mimetics, of which one faces the outer leaflet and the other the inner leaflet of the lipid bilayer.[42,43] Although the two FFAR1 sites in the X-ray structures were occupied by two different synthetic lipid mimetics, they potentially both serve as binding sites for endogenous LCFA ligands,[44] and radioligand binding experiments with site-selective synthetic ligands have demonstrated strong positive cooperativity between the two sites.[45] In the case of SUCNR1, our metadynamics simulations demonstrate low-energy binding of succinate in each of the two sites. This indicates that succinate has a relatively high and rather similar affinity for both sites, which, likely, is at least similar to acetylcholine and catecholamines in their respective receptors. However, although SUCNR1 is highly specific for succinate, its potency is in the micro- to millimolar range as often is the case for metabolite receptors[1] The explanation for how SUCNR1 can recognize succinate with low affinity, but still, high selectivity, is likely that both of its high-affinity sites need to be occupied at the same time for the receptor to be activated. In such a scenario, the

second succinate molecule needs to bind before the first has left the receptor.

Agonist binding in the orthosteric site is always associated with the release of constrained ECL-2b

It was early on realized that ECL-2b in most family A GPCRs functions as a "lid" over the main ligand binding pocket often with key interactions with the more deeply bound ligands.[46,47] Here, we find that ECL-2b probably plays an important role in the activation mechanism of SUCNR1. Thus, in all our unbiased MD simulations where a succinate or CES molecule moved down to bind in the deep orthosteric site, the passage of the agonist broke the constraining $D170^{45.52}$ to $Y272^{7.35}$ H-bond and thereby released the conformationally constrained ECL-2b. Our analysis of water movements indicated that a water cluster between the two carboxylates of succinate in its *cis* conformation likely is responsible for this breakage, which could explain why we did not observe breakage of this H-bond in connection with binding of the mono-carboxylate antagonist NF-56-EJ40 to the same deep site. Based on these observations, we propose that the liberation of ECL-2b and thereby the breakage of the tight packing between the neighboring TM-VI and -VII and the TMs on the "other" side of the seven helical bundles (Figure 4B) is a critical component in the activation process for SUCNR1. Importantly, in several other GPCRs, breakage of a similar bond between a residue located close to the conserved Cys in ECL-2 and a residue on the inner face of TM-VII has been demonstrated to be associated with agonist binding and receptor activation as shown by nuclear magnetic resonance and X-ray crystallography. This is the case, for the β1 adrenergic receptor, the SUCNR1-related P2y1 receptor,[48] the histamine H4 receptor,[49] and even in rhodopsin.[50] Moreover, the very high constitutive activity of the ghrelin receptor has been shown to be totally dependent on a high degree of flexibility of ECL-2b.[51] Thus, although the structural details may vary between receptors in respect of type and precise location of the constraining bond(s), a picture is emerging where receptor activation—be it constitutive or agonist mediated—is associated with breakage of conformationally constraining bond(s) between a residue located closely after the conserved Cys in ECL-2b, i.e., close to the top of TM-III, and a residue at the top of TM-VII. In most cases the unlocking of ECL-2b represents a classical Koshland type of induced fit allostery because it is closely associated to the actual agonist binding event.

Potential impact on discovery and design of pharmacological SUCNR1 ligands

SUCNR1 clearly plays an important role as a sensor of metabolic stress,[4,5] and as such, the receptor is physiologically involved in tissue repair and remodeling, as well as in pathophysiological inflammation and fibrosis, e.g., in nonalcoholic steatohepatitis (NASH).[6,7] However, unfortunately, there are still only a few useful pharmacological tool compounds available for SUCNR1. For example, although NF-56-EJ40 is a relatively potent antagonist, it is totally human selective and has rather poor drug metabolism and pharmacokinetics (DMPKs) properties, making it rather useless in, e.g., rodent animal models, which are important in early drug discovery.[24] In respect of SUCNR1 agonists, we have previously identified a series of backbone-modified succinate analogs with amide-linked aromatic side chains,[26] which, however, turned out only to be partial, mainly Gi-biased agonists.[27]

Our MD simulations based on the high-resolution SUCNR1 structures now provide a resource of both agonist-bound and antagonist-bound receptor binding pocket conformations to generate useful ensembles of receptor structures as templates for virtual screens and compound docking. The power of this approach is illustrated in the recent discovery of a class of novel, non-lipid-like FFAR1/GPR40 agonists specifically targeting a dynamic pocket, which—importantly—is only observed/open in the active receptor conformation.[31] In SUCNR1 ensembles of receptor structures where ECL-2b is unlocked, i.e., conceivably biased toward overall active receptor conformations could be used in virtual screens aiming at discovering novel agonists. With respect to the antagonist, our MD analysis underscores the notion that not only residues of the final binding pocket but also residues in the ligand entry path can be important for the compound activity—in this case, illustrated by the residue in position 18 of SUCNR1 being important for the species selectivity of the antagonist. Such information can be used in future virtual screens and/or in subsequent funneling and selection of compounds in the drug discovery process not only in SUCNR1 but in general.

Limitations of the study

Although (1) the metadynamics analysis demonstrates that both the orthosteric and the ECV site are low-energy succinate binding sites, (2) the multiple unbiased MD simulations demonstrate that dual, simultaneous occupancy of these two sites is a frequent endpoint, and (3) mutagenesis show that both the orthosteric and the distant ECV site are required for receptor activation, we do not directly demonstrate that simultaneous occupancy of both sites is required for receptor activation. This favored notion could potentially be further substantiated—but not really proven—by, e.g., radioligand binding experiments.

A general, major limitation of the unbiased MD simulations is their relatively short duration, which limits studies of conformational changes of the intracellular domain associated with activation and G protein binding. However, although we do observe indications of opening of the cleft between TM3 and −6 in a subset of simulations (unpublished data), the experimental setup was not designed to study these events because we, for example, observe intermittent succinate interactions with basic residues at the intracellular domain. These are not necessarily unphysiological events because succinate during metabolic stress is found in high concentrations also intracellularly, but this and other intracellular factors need to be better controlled.

Cryo-EM structures of SUCNR1, in complex with succinate, could potentially give the answer, i.e., whether it will be possible to obtain structures with either one or two succinate molecules bound.

STAR★METHODS

Detailed methods are provided in the online version of this paper and include the following:

SUPPLEMENTAL INFORMATION

Supplemental information can be found online at https://doi.org/10.1016/j.molcel.2024.01.011.

ACKNOWLEDGMENTS

The authors would like to thank Anja A. Petersen for expert technical assistance and Florent Smit for his advisory on the use of FindWaters.py. A.S. is the recipient of a fellowship from the Novo Nordisk Foundation as part of the Copenhagen Bioscience PhD Programme, supported through grant NNF19SA0035442. The Novo Nordisk Foundation Center for Basic Metabolic Research (CBMR) is supported by an unconditional grant NNF10CC1016515 from the Novo Nordisk Foundation (NNF) to University of Copenhagen. The work was furthermore supported by an Immunometabolism grant NNF15CC0018346 from the Novo Nordisk Foundation (T.W.S.). E.P. group is supported by Danmarks Grundforskningsfond (DNRF125) and NovoNordisk Fonden Bioscience and Basic Biomedicine (NNF20OC0065262).

AUTHOR CONTRIBUTIONS

A.S., M. Lückmann, T.M.F., and T.W.S. conceived the project and designed the research. A.S. performed molecular modeling. A.S. performed and analyzed MD simulations. A.S. performed molecular pharmacological experiments. M. Lückmann and A.S. performed water cluster analysis. A.S., M. Lambrughi, M. Tiberti, and E.P. contributed to insight performing metadynamics and analyzing data. The manuscript was written by T.W.S. and A.S. with critical review and input from all authors.

DECLARATION OF INTERESTS

M. Trauelsen, T.M.F., and T.W.S. are co-founders of SOLID Therapeutics, and T.W.S. is a co-founder of Embark Biotech.

Received: April 6, 2023
Revised: November 30, 2023
Accepted: January 16, 2024
Published: February 6, 2024

REFERENCES

1. Husted, A.S., Trauelsen, M., Rudenko, O., Hjorth, S.A., and Schwartz, T.W. (2017). GPCR-Mediated Signaling of Metabolites. Cell Metab. *25*, 777–796.
2. He, W., Miao, F.J.P., Lin, D.C.H., Schwandner, R.T., Wang, Z., Gao, J., Chen, J.L., Tian, H., and Ling, L. (2004). Citric acid cycle intermediates as ligands for orphan G-protein-coupled receptors. Nature *429*, 188–193.
3. Fernández-Veledo, S., Ceperuelo-Mallafré, V., and Vendrell, J. (2021). Rethinking succinate: an unexpected hormone-like metabolite in energy homeostasis. Trends Endocrinol. Metab. *32*, 680–692.
4. Murphy, M.P., and Chouchani, E.T. (2022). Why succinate? Physiological regulation by a mitochondrial coenzyme Q sentinel. Nat. Chem. Biol. *18*, 461–469.
5. Winther, S., Trauelsen, M., and Schwartz, T.W. (2021). Protective succinate-SUCNR1 metabolic stress signaling gone bad. Cell Metab. *33*, 1276–1278.
6. Trauelsen, M., Hiron, T.K., Lin, D., Petersen, J.E., Breton, B., Husted, A.S., Hjorth, S.A., Inoue, A., Frimurer, T.M., Bouvier, M., et al. (2021). Extracellular succinate hyperpolarizes M2 macrophages through SUCNR1/GPR91-mediated Gq signaling. Cell Rep. *35*, 109246.
7. Mills, E.L., Harmon, C., Jedrychowski, M.P., Xiao, H., Garrity, R., Tran, N.V., Bradshaw, G.A., Fu, A., Szpyt, J., Reddy, A., et al. (2021). UCP1 governs liver extracellular succinate and inflammatory pathogenesis. Nat. Metab. *3*, 604–617.
8. Villanueva-Carmona, T., Cedó, L., Madeira, A., Ceperuelo-Mallafré, V., Rodríguez-Peña, M.M., Núñez-Roa, C., Maymó-Masip, E., Repollés-de-Dalmau, M., Badia, J., Keiran, N., et al. (2023). SUCNR1 signaling in adipocytes controls energy metabolism by modulating circadian clock and leptin expression. Cell Metab. *35*, 601–619.e10.
9. García-Nafría, J., and Tate, C.G. (2021). Structure determination of GPCRs: cryo-EM compared with X-ray crystallography. Biochem. Soc. Trans. *49*, 2345–2355.
10. Kimura, K.T., Asada, H., Inoue, A., Kadji, F.M.N., Im, D., Mori, C., Arakawa, T., Hirata, K., Nomura, Y., Nomura, N., et al. (2019). Structures of the 5-HT2A receptor in complex with the antipsychotics risperidone and zotepine. Nat. Struct. Mol. Biol. *26*, 121–128.
11. Koehl, A., Hu, H., Maeda, S., Zhang, Y., Qu, Q., Paggi, J.M., Latorraca, N.R., Hilger, D., Dawson, R., Matile, H., et al. (2018). Structure of the μ-opioid receptor-G_i protein complex. Nature *558*, 547–552.
12. Wang, J., Wu, M., Chen, Z., Wu, L., Wang, T., Cao, D., Wang, H., Liu, S., Xu, Y., Li, F., et al. (2022). The unconventional activation of the muscarinic acetylcholine receptor M4R by diverse ligands. Nat. Commun. *13*, 2855.
13. Schwartz, T.W., and Rosenkilde, M.M. (1996). Is there a 'lock' for all agonist 'keys' in 7TM receptors? Trends Pharmacol. Sci. *17*, 213–216.
14. Monod, J., Wyman, J., and Changeux, J.P. (1965). On the nature of allosteric transitions: A plausible model. J. Mol. Biol. *12*, 88–118.
15. Schwartz, T.W., Frimurer, T.M., Holst, B., Rosenkilde, M.M., and Elling, C.E. (2006). MOLECULAR MECHANISM OF 7TM RECEPTOR ACTIVATION—A GLOBAL TOGGLE SWITCH MODEL. Annu. Rev. Pharmacol. Toxicol. *46*, 481–519.
16. Latorraca, N.R., Venkatakrishnan, A.J., and Dror, R.O. (2017). GPCR Dynamics: Structures in Motion. Chem. Rev. *117*, 139–155.
17. Karplus, M., and McCammon, J.A. (2002). Molecular dynamics simulations of biomolecules. Nat. Struct. Biol. *9*, 646–652.
18. Hollingsworth, S.A., and Dror, R.O. (2018). Molecular Dynamics Simulation for All. Neuron *99*, 1129–1143.
19. Dror, R.O., Pan, A.C., Arlow, D.H., Borhani, D.W., Maragakis, P., Shan, Y., Xu, H., and Shaw, D.E. (2011). Pathway and mechanism of drug binding to G-protein-coupled receptors. Proc. Natl. Acad. Sci. USA *108*, 13118–13123.
20. Kruse, A.C., Hu, J., Pan, A.C., Arlow, D.H., Rosenbaum, D.M., Rosemond, E., Green, H.F., Liu, T., Chae, P.S., Dror, R.O., et al. (2012). Structure and dynamics of the M3 muscarinic acetylcholine receptor. Nature *482*, 552–556.
21. Dror, R.O., Green, H.F., Valant, C., Borhani, D.W., Valcourt, J.R., Pan, A.C., Arlow, D.H., Canals, M., Lane, J.R., Rahmani, R., et al. (2013). Structural basis for modulation of a G-protein-coupled receptor by allosteric drugs. Nature *503*, 295–299.
22. Kappel, K., Miao, Y., and McCammon, J.A. (2015). Accelerated molecular dynamics simulations of ligand binding to a muscarinic G-protein-coupled receptor. Q. Rev. Biophys. *48*, 479–487.
23. Xu, X., Kaindl, J., Clark, M.J., Hübner, H., Hirata, K., Sunahara, R.K., Gmeiner, P., Kobilka, B.K., and Liu, X. (2021). Binding pathway determines

norepinephrine selectivity for the human beta1AR over beta2AR. Cell Res. *31*, 569–579.

24. Haffke, M., Fehlmann, D., Rummel, G., Boivineau, J., Duckely, M., Gommermann, N., Cotesta, S., Sirockin, F., Freuler, F., Littlewood-Evans, A., et al. (2019). Structural basis of species-selective antagonist binding to the succinate receptor. Nature *574*, 581–585.
25. Geubelle, P., Gilissen, J., Dilly, S., Poma, L., Dupuis, N., Laschet, C., Abboud, D., Inoue, A., Jouret, F., Pirotte, B., et al. (2017). Identification and pharmacological characterization of succinate receptor agonists. Br. J. Pharmacol. *174*, 796–808.
26. Trauelsen, M., Rexen Ulven, E., Hjorth, S.A., Brvar, M., Monaco, C., Frimurer, T.M., and Schwartz, T.W. (2017). Receptor structure-based discovery of non-metabolite agonists for the succinate receptor GPR91. Mol. Metab. *6*, 1585–1596.
27. Rexen Ulven, E., Trauelsen, M., Brvar, M., Lückmann, M., Bielefeldt, L.Ø., Jensen, L.K.I., Schwartz, T.W., and Frimurer, T.M. (2018). Structure-Activity Investigations and Optimisations of Non-metabolite Agonists for the Succinate Receptor 1. Sci. Rep. *8*, 10010.
28. Velcicky, J., Wilcken, R., Cotesta, S., Janser, P., Schlapbach, A., Wagner, T., Piechon, P., Villard, F., Bouhelal, R., Piller, F., et al. (2020). Discovery and Optimization of Novel SUCNR1 Inhibitors: Design of Zwitterionic Derivatives with a Salt Bridge for the Improvement of Oral Exposure. J. Med. Chem. *63*, 9856–9875.
29. Zhang, D., Gao, Z.G., Zhang, K., Kiselev, E., Crane, S., Wang, J., Paoletta, S., Yi, C., Ma, L., Zhang, W., et al. (2015). Two disparate ligand-binding sites in the human P2Y1 receptor. Nature *520*, 317–321.
30. Rosenbaum, D.M., Rasmussen, S.G., and Kobilka, B.K. (2009). The structure and function of G-protein-coupled receptors. Nature *459*, 356–363.
31. Lückmann, M., Trauelsen, M., Bentsen, M.A., Nissen, T.A.D., Martins, J., Fallah, Z., Nygaard, M.M., Papaleo, E., Lindorff-Larsen, K., Schwartz, T.W., et al. (2019). Molecular dynamics-guided discovery of an ago-allosteric modulator for GPR40/FFAR1. Proc. Natl. Acad. Sci. USA *116*, 7123–7128.
32. Burger, W.A.C., Pham, V., Vuckovic, Z., Powers, A.S., Mobbs, J.I., Laloudakis, Y., Glukhova, A., Wootten, D., Tobin, A.B., Sexton, P.M., et al. (2023). Xanomeline displays concomitant orthosteric and allosteric binding modes at the M4 mAChR. Nat. Commun. *14*, 5440.
33. Conrad, M., Söldner, C.A., Miao, Y., and Sticht, H. (2020). Agonist Binding and G Protein Coupling in Histamine H_2 Receptor: A Molecular Dynamics Study. Int. J. Mol. Sci. *21*, 6693.
34. Thomas, T., Fang, Y., Yuriev, E., and Chalmers, D.K. (2016). Ligand Binding Pathways of Clozapine and Haloperidol in the Dopamine D2 and D3 Receptors. J. Chem. Inf. Model. *56*, 308–321.
35. Do, H.N., Akhter, S., and Miao, Y. (2021). Pathways and Mechanism of Caffeine Binding to Human Adenosine A2A Receptor. Front. Mol. Biosci. *8*, 673170.
36. Honig, B., and Nicholls, A. (1995). Classical Electrostatics in Biology and Chemistry. Science *268*, 1144–1149.
37. Miao, Y., Bhattarai, A., and Wang, J. (2020). Ligand Gaussian Accelerated Molecular Dynamics (LiGaMD): Characterization of Ligand Binding Thermodynamics and Kinetics. J. Chem. Theory Comput. *16*, 5526–5547.
38. Bhattarai, A., and Miao, Y. (2018). Gaussian accelerated molecular dynamics for elucidation of drug pathways. Expert Opin. Drug Discov. *13*, 1055–1065.
39. Faouzi, A., Wang, H., Zaidi, S.A., DiBerto, J.F., Che, T., Qu, Q., Robertson, M.J., Madasu, M.K., El Daibani, A., Varga, B.R., et al. (2023). Structure-based design of bitopic ligands for the μ-opioid receptor. Nature *613*, 767–774.
40. Decker, M., Fulton, B.S., Zhang, B., Knapp, B.I., Bidlack, J.M., and Neumeyer, J.L. (2009). Univalent and Bivalent Ligands of Butorphan: Characteristics of the Linking Chain Determine the Affinity and Potency of Such Opioid Ligands. J. Med. Chem. *52*, 7389–7396.
41. Zhang, B., Zhang, T., Sromek, A.W., Scrimale, T., Bidlack, J.M., and Neumeyer, J.L. (2011). Synthesis and binding affinity of novel mono- and bivalent morphinan ligands for κ, μ, and δ opioid receptors. Bioorg. Med. Chem. *19*, 2808–2816.
42. Srivastava, A., Yano, J., Hirozane, Y., Kefala, G., Gruswitz, F., Snell, G., Lane, W., Ivetac, A., Aertgeerts, K., Nguyen, J., et al. (2014). High-resolution structure of the human GPR40 receptor bound to allosteric agonist TAK-875. Nature *513*, 124–127.
43. Ho, J.D., Chau, B., Rodgers, L., Lu, F., Wilbur, K.L., Otto, K.A., Chen, Y., Song, M., Riley, J.P., Yang, H.C., et al. (2018). Structural basis for GPR40 allosteric agonism and incretin stimulation. Nat. Commun. *9*, 1645.
44. Lückmann, M., Trauelsen, M., Frimurer, T.M., and Schwartz, T.W. (2020). Structural basis for GPCR signaling by small polar versus large lipid metabolites—discovery of non-metabolite ligands. Curr. Opin. Cell Biol. *63*, 38–48.
45. Hauge, M., Vestmar, M.A., Husted, A.S., Ekberg, J.P., Wright, M.J., Di Salvo, J., Weinglass, A.B., Engelstoft, M.S., Madsen, A.N., Lückmann, M., et al. (2015). GPR40 (FFAR1) - Combined Gs and Gq signaling in vitro is associated with robust incretin secretagogue action ex vivo and in vivo. Mol. Metab. *4*, 3–14.
46. Nygaard, R., Frimurer, T.M., Holst, B., Rosenkilde, M.M., and Schwartz, T.W. (2009). Ligand binding and micro-switches in 7TM receptor structures. Trends Pharmacol. Sci. *30*, 249–259.
47. Wheatley, M., Wootten, D., Conner, M.T., Simms, J., Kendrick, R., Logan, R.T., Poyner, D.R., and Barwell, J. (2012). Lifting the lid on GPCRs: the role of extracellular loops. Br. J. Pharmacol. *165*, 1688–1703.
48. Li, Y., Yin, C., Liu, P., Li, D., and Lin, J. (2017). Identification of a Different Agonist-Binding Site and Activation Mechanism of the Human P2Y1 Receptor. Sci. Rep. *7*, 13764.
49. Wifling, D., Bernhardt, G., Dove, S., and Buschauer, A. (2015). The Extracellular Loop 2 (ECL2) of the Human Histamine H4 Receptor Substantially Contributes to Ligand Binding and Constitutive Activity. PLoS One *10*, e0117185.
50. Ahuja, S., Hornak, V., Yan, E.C., Syrett, N., Goncalves, J.A., Hirshfeld, A., Ziliox, M., Sakmar, T.P., Sheves, M., Reeves, P.J., et al. (2009). Helix movement is coupled to displacement of the second extracellular loop in rhodopsin activation. Nat. Struct. Mol. Biol. *16*, 168–175.
51. Mokrosiński, J., Frimurer, T.M., Sivertsen, B., Schwartz, T.W., and Holst, B. (2012). Modulation of constitutive activity and signaling bias of the ghrelin receptor by conformational constraint in the second extracellular loop. J. Biol. Chem. *287*, 33488–33502.
52. Jiang, L.I., Collins, J., Davis, R., Lin, K.M., DeCamp, D., Roach, T., Hsueh, R., Rebres, R.A., Ross, E.M., Taussig, R., et al. (2007). Use of a cAMP BRET sensor to characterize a novel regulation of cAMP by the sphingosine 1-phosphate/G13 pathway. J. Biol. Chem. *282*, 10576–10584.
53. Humphrey, W., Dalke, A., and Schulten, K. (1996). VMD: Visual molecular dynamics. J. Mol. Graph. *14*, 33–38.
54. Hunter, J.D. (2007). Matplotlib: A 2D Graphics Environment. Comput. Sci. Eng. *9*, 90–95.
55. Sakai, Y., Kawaguchi, A., Nagata, K., and Hirokawa, T. (2018). Analysis by metadynamics simulation of binding pathway of influenza virus M2 channel blockers. Microbiol. Immunol. *62*, 34–43.
56. Smit, F.X., van der Velden, W.J.C., Kizilkaya, H.S., Nørskov, A., Lückmann, M., Hansen, T.N., Sparre-Ulrich, A.H., Qvotrup, K., Frimurer, T.M., and Rosenkilde, M.M. (2021). Investigating GIPR (ant)agonism: A structural analysis of GIP and its receptor. Structure *29*, 679–693.e6.

STAR★METHODS

KEY RESOURCES TABLE

REAGENT or RESOURCE	SOURCE	IDENTIFIER
Chemicals, peptides, and recombinant proteins		
Sodium succinate dibasic	Sigma-Aldrich	Product: 14160 CAS: 150-90-3
YSi SPA scintillation beads	PerkinElmer	Cat# RPNQ0010
Co-elenterazine h	ThermoFisher	Cat# C6780 CAS: 50909-86-9
HBSS	Gibco	Cat# 14025050
myo [^{3}H]inositol	PerkinElmer	Cat# NET114A005MC
DMEM 1885	Gibco	Cat# 11885-084
DMEM 1966	Gibco	Cat# 31966-021
PBS	Substrate Department – UCPH	N/A
Trypsin	Bioscience	Cat# BE17-161E
NF-56-EJ40	Targetmol	Catalog# T12216 CAS:2380230-73-7
Critical commercial assays		
QuikChange II Site-Directed Mutagenesis Kit	Agilent	Cat# 200523
NucleoBond Xtra Midi kit	Macherey-Nagel	Cat# 740410.100
Deposited data		
Simulation trajectories of ligand binding to SUCNR1	https://doi.org/10.5281/zenodo.10213670	https://www.zenodo.org
Experimental models: Cell lines		
XL1-Blue Competent Cells	Agilent	Cat# 200228
Cos 7 Cells	ATCC	ATCC® CRL-1651
Recombinant DNA		
Murine SUCNR1 construct	Origene	MR204545
Human SUCNR1 construct	Origene	RC205888
CAMYEL	Jiang et al.[52]	N/A
Software and algorithms		
ICM-Pro	MolSoft LLC	https://www.molsoft.com/
Prime	Schrödinger, Inc.	https://www.schrodinger.com/products/prime
Maestro	Schrödinger, Inc.	https://www.schrodinger.com/products/maestro
Desmond	Schrödinger, Inc.	https://www.schrodinger.com/products/desmond
PyMOL	Schrödinger, Inc.	https://pymol.org/
VMD	Humphrey et al.[53]	http://www.ks.uiuc.edu/Research/vmd/
Matplotlib	Hunter et al.[54]	https://matplotlib.org/1.2.1/index.html
Prism	GraphPad, Inc.	https://www.graphpad.com/scientific-software/prism/
MicroBeta 2 Workstation	Perkin Elmer	https://www.perkinelmer.com/uk/product/microbeta2-plate-reader-with-1-detector/
MARS Data Analysis Software	BMG LABTECH	https://www.bmglabtech.com/en/microplate-reader-software/

RESOURCE AVAILABILITY

Lead contact

Further information and requests for reagents should be directed to and will be fulfilled by the lead contact, Thue W. Schwartz (tws@sund.ku.dk).

Materials availability

This study did not generate new unique reagents.

Data and code availability

- Trajectories generated and used for this manuscript are deposited on Zenodo and are publicly available as of the date of publication. DOIs are listed in the key resources table.
- This study did not generate any original code.
- Any additional information and trajectories required to reanalyze the data reported in this paper are available from the lead contact upon request.

EXPERIMENTAL MODEL AND STUDY PARTICIPANT DETAILS

Cell culture and transfection

All experiments were conducted on COS7 cell line (African green monkey kidney fibroblast-like cell line) were maintained in Dulbecco's modified Eagle's medium 21885 (DMEM) supplemented with 10 % fetal bovine serum, 2 mM glutamine, 100 units/ml penicillin, and 100 μg/ml streptomycin at 37°C with 10% CO_2. cells were grown in Dulbecco's modified Eagle's medium 21885 (DMEM) supplemented with 10 % fetal bovine serum, 2 mM glutamine, 100 units/ml penicillin, and 100 μg/ml streptomycin. For IP accumulation and cAMP assays, 20,000 cells/well were cultured overnight in 96-well plates and subsequently transiently transfected (400ng DNA/well) using the calcium phosphate precipitation method with chloroquine addition. The medium was replaced after 5h of incubation. For the IP accumulation assay, the cells were incubated overnight in 100 μl growth medium with 0.5 μCi/ml myo[3H] inositol (IP accumulation) or without (cAMP).

METHOD DETAILS

COMPUTATIONAL METHOD

Receptor Structure Preparation

Simulations of SUCNR1 were based on the humanized rat SUCNR1 (GPR91) crystal structure (PDB: 6rnk). For some of the simulations (see Table S1) the humanized rat SUCNR1 structure – PDB:6z10 and the rat SUNR1 crystal structure (PDB: 6ibb) were used. The structure was prepared by removing nanobody 6 and the antagonist molecule NF-56-EJ40. Residues C7 and L305 were capped with acetyl groups (ACE) and N-methyl amide (NMA), respectively. Side chains that were not resolved in the structure (i.e. intracellular loop 3, ICL3, and part of extracellular loop 2, ECL2) were modeled using Prime (Schrödinger) and were subsequently refined. Hydrogen atoms were added using the Protein Preparation Wizard workflow in Maestro (Schrödinger), and bond orders were assigned. Since we removed the co-crystallized ligand, we removed all water molecules. Histidine residues were modeled as neutral. The hydrogens were optimized and minimized using PROPKA for pH 7.0 and the heavy atoms were set to converge to RMSD 0.3 Å, using the OPLSe3 force field For receptor preparation, system setup, and simulations we used Schrödinger Release 2019-4: Maestro, Schrödinger, LLC, New York, NY, 2019.

Simulation System Setup

The prepared GPR91 structure was inserted into a predefined POPC bilayer preequilibrated at 300K. The water solvent model TIP3P was used. Ten ligand molecules (succinate or CES) were placed randomly at least 14 Å above the ECV in the bulk solvent. The ligands were parametrized via the ForceField Builder using the OPLSe3 force field and ionization states were generated for the same pH values 7.0 +/- 2.0, using LigPrep, and Epik. The maximum ligand size was set to 500 atoms and possible combinations of chirality were generated. Succinate's pK_a was calculated to be 3.31 (CES pK_a = 3.92), and both carboxylic ends were therefore deprotonated. Sodium ions were added to neutralize each system. Periodic boundary conditions were applied to all systems. The system was built using an orthorhombic box shape with 10 Å buffer distance between the solute structures and the simulation boundary box. The simulation system measured about 72 x 80 x 104 Å. The whole system comprised approximately 60.000 atoms in total with approximately 110 lipid molecules, 10.200 water molecules, and 10 sodium ions. The customized force field (OPLSe3) was used throughout the simulations.

Additionally, we have performed 13 simulations for 1000-2000 ns in the presence of 33 sodium and 33 chloride ions corresponding to 0.15 M NaCl plus 10 extra Na ions to neutralize the system. Results from these new simulations are shown in Table S4 and Figures S8 and S9. The dynamics of succinate binding was very similar to that observed without the extra sodium and chloride ions present and the same ligand binding modes were observed.

Molecular Dynamics simulations

The Desmond simulations simulated in the NPγT ensemble at 310 K, 1 bar applying a surface tension of 4000 bar.Å. The Desmond minimization protocol uses the steepest descent method. The protocol includes restrained followed by non-restrained equilibration steps, each running for 5 ns. During the equilibration process, the cutoff for *van der Waals* and short-range electrostatic interactions was set to 9 Å. RESPA integrator was used with a time step of 2 fs, and long-range electrostatics were computed every 6 fs. The system was equilibrated in the NVT ensemble for 100 ps using Brownian dynamics with T=10K and 50 kcal/mol/Å^2. restrains applied on solute heavy atoms. This was followed by an Brownian equilibration in the NPT ensemble at T = 50K and a H_2O barrier and restraints (force constant=5 kcal/mol/Å^2.) applied on the membrane in the z-direction and the protein. Finally, the system was equilibrated in the NPγT ensemble at T= 50K using the same restraints, followed by gradual heating from 100 to 300K, using a H_2O barrier and gradual release of the restrains. This was followed by two NVT production steps with all restrains removed. The final production simulations were performed after a brief minimization. For the simulation, the customized OPLSe3 force field was used. As a housekeeping metric, the first 50ns of the simulations were not included in the analysis.

Simulation Analysis

Generated trajectories were visualized using Maestro and analyzed using Simulation Interaction Diagram, Simulation Event Analysis and VMD.[53] Data were visualized using GraphPad Prism (GraphPad Software) and Matplotlib (version 3.5.2), Python (version 3.8.18).[54] Visualization of protein structures and trajectory frames was done on PyMOL (PyMOL Molecular Graphics System, Version 1.2r3pre, Schrödinger, LLC) and VMD (version 1.9.4a57).

Homology modeling

The homology model of the inactive state of human SUCNR1 and murine SUCNR1 was constructed using ICM 3.8(Molsoft L.L.C. 11199 Sorrento Valley Road, S209 San Diego CA92121) based on the available humanized rat and rat GPR91 crystal structures. The model was relaxed using 500 steps of Cartesian minimization, followed by a global side-chain minimization (500 moves). The generated model was further processed using Protein Preparation Wizard, Schrödinger, as described above, to determine optimal protonation states for histidine residues and correct potentially transposed heavy atoms in residue side chains.

Well-tempered Metadynamics

Well-tempered metadynamics was used to investigate the free energy landscapes and the binding of succinate and antagonists to GPR91 (PDB:6rnk). The system was prepared as previously described. One ligand molecule was placed above the receptor's extracellular plane, at a distance of at least 28 Å of F280. Setup conditions for the simulations were as described by Sakai et al.[55] To ensure the successful implementation of well-tempered metadynamics using Desmond (Schrödinger, LLC) under the specified conditions, our primary references were the Desmond User Manual and Sakai et al.[55] We used a customized OPLSe3 force field for the metadynamics simulation. For biasing collective variables, we specifically chose the distance between the center of masses for succinate and the center of masses for F280. Multiple independent simulations were conducted using Desmond (Schrödinger, LLC). The ligand entry into the receptor and its poses in the binding pockets were examined and compared to the unbiased MD initially performed. In the presented replica, we consistently observed the ligand entering between TM-VI and TM-VII, along with interactions with both the ECV and the orthosteric binding site.

To ensure the accuracy of the simulation, several parameters were considered. These include the height and width of the Gaussian potential, as well as the interval between adding Gaussians. The width of the Gaussian generally ranged from approximately 1/4 or 1/5 of the average fluctuations observed in the collective variable during an unbiased molecular dynamics trajectory. Based on our simulations, we determined that the standard deviation for the distance between the center of masses for F280 and succinate in its bound state was 0.27 Å. Consequently, we chose a Gaussian width value of 0.05. Our research indicated that reducing the height/interval ratio improved accuracy. Therefore, we opted for an interval of 0.09ps. The height of the repulsive Gaussian was set to 0.1. It is worth noting that the accuracy of results decreases with increasing height for a given interval of adding Gaussians. However, choosing smaller heights would lengthen the simulations. Therefore, we identified 0.1 as the optimal value.

Since our collective variable is distance, we introduced a wall to restrict the system from moving excessively in the direction defined by the collective variable. The well-tempered parameter was set to 2.4 kcal/mol as suggested in our references. Ensemble class NPγT as described and default relaxation protocol is implemented as described above. Data were analyzed using the Metadynamics Analysis tool, Simulation Event Analysis, and Simulation Interaction Diagram, Maestro, Schrödinger.

Water clusters analysis

Conserved water molecules were found using FindWaters.py (available on GitHub, https://github.com/florent411/FindWaters.py). This algorithm is based on doing a kernel density estimation (kde) on all oxygen atoms that are found in a spherical binding pocket throughout all frames of the equilibrated part of the molecular dynamic simulation. The highest-density regions, with a cumulative sum of 10% probability, were saved and clustered using the KMeans clustering algorithm.[56]

BIOLOGICAL METHODS

IP accumulation assay

The inositol phosphate (IP) accumulation assay is employed to indirectly determine the increase in inositol 1,4,5-triphosphate (IP3) levels in cells following stimulation by an agonist. In this assay, the degradation of IP2 and IP is inhibited, if the total soluble IP mass in the cell originates from the breakdown of IP3. To achieve this, lithium ions (Li+) are added to the assay buffer, effectively blocking the activity of inositol polyphosphate-1-phosphatase (IPPase) and inositol monophosphatase (IMPase). This inhibition results in the

accumulation of IP and IP2, which serve as indicators of IP3 accumulation. Additionally, the inclusion of [3H] Myo-inositol allows for the incorporation of radiolabel into phosphatidylinositol 4,5-bisphosphate (PIP2) in the cell membrane, functioning as a tracer. The transfected cells are washed with 200 μl/well HBSS (Gibco, Life Technologies), and 100 μl of HBSS with 10mM LiCl are added before the tested ligands. Ligands were added as dose-response curves followed by 90 minutes of incubation at 37°C. After incubation, cells were lysed with 40 μl ice-cold 10 mM formic acid and incubated on ice for 45 minutes. 35 μl from each well were transferred to a white 96-well plate with 60 μl of 1:8 diluted YSi poly-d-lysine coated beads (Perkin Elmer). After shaking and centrifugation at 1500rpm for 5min, light emission was recorded on a Microbeta (PerkinElmer)after a 4 h delay. Determinations were made in triplicates.

cAMP (BRET) assay

The level of cAMP-dependent on the Gi signaling of SUCNR1 was determined by using bioluminescence resonance energy transfer (BRET) as described in Trauelsen et al.[6] This approach relies on a structure comprising a BRET pair (Renilla luciferase (Rluc) and yellow fluorescent protein (YFP)) that surrounds a cAMP binding protein called Exchange protein activated by cAMP (Epac). The whole complex is called CAMYEL[52](cAMP sensor using YFP-Epac-Rluc). As cAMP levels rise, the conformation of Epac changes, and this alteration is detected as a decrease in BRET intensity, indicating the production of cAMP. COS7 cells were plated in poly-D-lysine-coated white 96-well plates (20.000 cells/well). The following day, cells were transfected as described above. The next day, the cells were rinsed twice with 100 ml/well of HBSS (GIBCO, Life Technologies) and preincubated for 30 minutes at 37°C with 60 mL of HBSS. Luciferase substrate coelenterazine (ThermoFisher) was added and after a 5 min incubation, a baseline was measured. Forskolin (10 mM) was used to activate adenylate cyclase and after ligands (dose-response curve dilutions) were added, measurements were recorded every 2 minutes for a total of 30 min on CLARIOstar® Plus plate reader. The resulting BRET signal is determined as a ratio of the emission intensities at 535 nm(citrine) and 475 nm (luciferase). Experiments were performed in triplicates and plotted as normalized values for the maximum value of cAMP inhibition of the wild type stimulated with the endogenous ligand.

Mutagenesis

The mGPR91 and hGPR91 receptor constructs were obtained from Origene and cloned into the eukaryotic expression vector pCMV-Tag (2B) (Stratagene). Point mutations were introduced by PCR using the QuickChange method. All PCR reactions were performed using Pfu polymerase (Stratagene) according to the manufacturer's instructions. DNA was purified from transformed cells carrying one specific point mutation with a midi prep kit from Qiagen. The constructs' DNA sequences were analyzed by GATC Biotech (GATC) (Constance, Germany).

QUANTIFICATION AND STATISTICAL ANALYSIS

In this study all cell signaling assay determinations were made in triplicates. Data is presented as mean ± standard error of the mean (SEM). Data was analyzed using GraphPad Prism (GraphPad Software) and non-linear regression, determining the Top and Bottom values, EC50 and HillSlope of the dose response curves.